





A low-symmetry nickel(II) α -diimine complex for homopolymerization of ethylene: study of interactive effects of polymerization parameters

Nona Ghasemi Hamedani, Hassan Arabi & Francis S. Mair

To cite this article: Nona Ghasemi Hamedani, Hassan Arabi & Francis S. Mair (2015) A low-symmetry nickel(II) α -diimine complex for homopolymerization of ethylene: study of interactive effects of polymerization parameters, Journal of Coordination Chemistry, 68:15, 2601-2619, DOI: [10.1080/00958972.2015.1057130](https://doi.org/10.1080/00958972.2015.1057130)

To link to this article: <http://dx.doi.org/10.1080/00958972.2015.1057130>

 View supplementary material 

 Accepted author version posted online: 02 Jun 2015.
Published online: 08 Jul 2015.

 Submit your article to this journal 

 Article views: 81

 View related articles 

 View Crossmark data 

A low-symmetry nickel(II) α -diimine complex for homopolymerization of ethylene: study of interactive effects of polymerization parameters

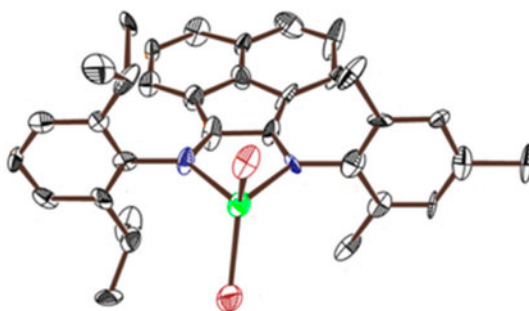
NONA GHASEMI HAMEDANI^{†§}, HASSAN ARABI^{*†} and FRANCIS S. MAIR^{*‡}

[†]Department of Polymerization Engineering, Iran Polymer and Petrochemical Institute, Tehran, Iran

[‡]School of Chemistry, The University of Manchester, Manchester, UK

[§]National Petrochemical Company (NPC), Research and Technology Company, Tehran, Iran

(Received 11 January 2015; accepted 2 May 2015)



In this contribution, the synthesis and characterization of a non-symmetric nickel(II) α -diimine complex [(2,4,6-trimethylphenyl)imino)-((2,6-diisopropylphenyl)imino)-acenaphthene nickel(II) dibromide] have been reported as a catalyst precursor for ethylene polymerization. Response surface method (RSM) has been applied successfully for investigation of operational conditions; it provides predictive models for activity, weight-average molecular weight (Mw), and crystallinity with adequate goodness of fit. The resultant activities challenge the best achieved with other unsymmetrical nickel (II) α -diimine systems. Considering the most critical factors and also their interactions on catalyst performance has been provided possibility to design final polymer characteristics. Further studies on nickel-catalyzed polymerizations may benefit from similar treatment of all relevant variables using RSM.

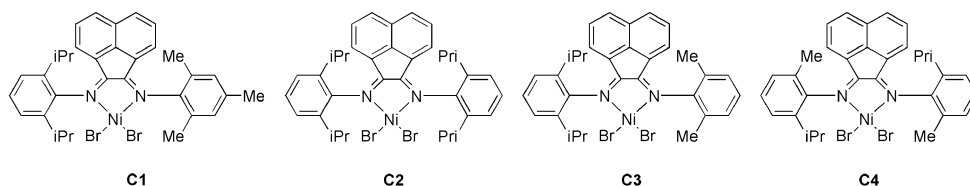
A low-symmetry nickel(II) α -diimine complex [(2,4,6-trimethylphenyl)imino)-((2,6-diisopropylphenyl)imino)-acenaphthene nickel(II) dibromide] (**C1**) was synthesized and characterized crystallographically. Response surface method (RSM) was employed to study the interactive effects of critical factors on ethylene polymerization. The maximum activity of **C1**, when activated by methylalumoxane (MAO) cocatalyst {4960 kgPE [(mol Ni)⁻¹ h⁻¹]} was achieved at 10 °C, 7 bar and CC (cocatalyst-to-catalyst ratio) equal to 1550, which is higher than most similar counterparts. Considering surface plots of MW, it is concluded that at high levels (>1000) of CC, there is competition between chain transfer to aluminum and reinsertion of macromonomer to newly formed metal-methyl bonds.

*Corresponding authors. Email: h.arabi@ippi.ac.ir (H. Arabi); francis.s.mair@manchester.ac.uk (F.S. Mair)

Keywords: Low-symmetry ligand; Nickel(II) α -diimine complex; Polyethylene (PE); Response surface method; Polymer properties

Introduction

The development of late transition metal complexes as catalysts for oligomerization and polymerization of α -olefins is of interest, mainly because of their air stability, polymerization characteristics, and tolerance to polar functional groups. A major advancement in this area was the discovery of homogeneous nickel and palladium α -diimine complexes in 1995 [1, 2]. Unique to these systems is the ability to yield a high degree of branching in the polyethylene produced without the use of α -olefin comonomers, a feature attributed to a catalytic mechanism referred to as “chain-walking” [3]. This mechanism is under the control of catalyst structure and polymerization conditions in such a way that properties of the polymer produced cover a wide range of grades from highly branched completely amorphous to semi-crystalline materials [3–5]. Tremendous efforts have been spent in both industrial and academic laboratories on improving late transition metal catalyst systems. Many structural modifications, including changing the ligand backbone structure or chelating heteroatoms, have been pursued on α -diimine systems [3, 6], since control of steric hindrance and ligand electronic structure is critical to the attainment of the desired properties in the catalytic system, and hence in the polymers produced from it. These parameters have been studied via modification of the ligand frameworks in two ways: (i) via variation of the substituents on the arylimino groups [4–15] and (ii) via changes in the backbone substituents [16–18]. As for (i), it has often been shown that the steric hindrances of *ortho* substituents affect the catalytic activity [11–13], where sufficient bulk retards the rate of associative olefin displacement, affording polymers with higher molecular weights, while electronic effects are also found for aryl substituents [9, 10, 12–15], whereas for (ii), it has also been shown that incorporation of electron-donating or electron-withdrawing substituents onto α -diimine ligand backbones affects their σ -donating ability to metal centers. This in turn affects the Lewis acidity of the metal [15–18], leading to effects on activities and selectivities of polymerization. An increase in polar olefin incorporation has been reported for electron-donating ligands [13–15], whereas *para*-chloro-substituents gave higher activities [9] than their hydro-equivalents. The effect of *p*-Me groups on aryls has been mixed, with reports of both higher [7] and lower [8] activities for *p*-Me versus *p*-H on aryl groups, dependent on organoaluminum and catalyst used. These reports employed a means to impart finer control on the degrees of bulk at the metal center through lowered symmetry [19, 20]. Catalyst **C1**, for example, lacks one of the molecular planes of symmetry present in benchmark C_{2v} -symmetry Brookhart catalyst **C2** [1], since it has different aryl groups on either side of the metal (scheme 1). Comparisons of activity for such a pairing have already been made in the literature [7], as have comparisons of the effect of *p*-Me groups and other remote electronic effects [7, 9, 10, 12–15], and of variations in the nature of the lowering of symmetry, e.g., in comparisons of **C4**, which retains a C_2 axis in the conformation shown, but which also possesses an alternative conformation where the plane of symmetry containing the C_2N_2Ni metallacycle is removed, whereas the plane of symmetry bisecting this plane, the one absent in **C1** and **C3**, is recovered (scheme 1) [19]. Interestingly, **C4**, with alternative conformations, gave a broader molecular weight distribution than



Scheme 1. Some nickel(II) α -diimine complexes with different symmetries.

its structural isomer **C3**, as well as higher molecular weight and lower branching density, demonstrating that even an identical set of ortho substituents, but differently arrayed, can generate different polymerization behaviors [19]. There are reports of polymerization activity for each of **C1**–**C4** already present in the literature [1, 7, 19], the area has been reviewed [21, 22], and a fundamental theoretical basis for the observations, which differ little from those of more symmetric cases, has been laid down [23–25]. However, reports of exhaustive and systematic study of the interplay of experimental conditions (temperature, pressure, cocatalyst ratio, etc.) with observed output parameters (branching rate, crystallinity, MW, etc.), the efficacy of which has recently been demonstrated for Ni(II)-catalyzed ethylene polymerizations [26], is absent for all diimine catalysts except **C2**, using Al^iBu_3 cocatalyst [27]. In this contribution, we apply response surface method (RSM) to **C1**, its first application in this area of lowered-symmetry Ni(II) α -diimine catalysts.

C1, bearing 2,6-diisopropylaniline on one side and 2,4,6-trimethylaniline on the other side, has been previously reported [7], though it was not structurally characterized. Its performance in ethylene polymerization was reported for a 30 min run at 10 bar ethylene pressure with CC 500, diethylaluminum chloride cocatalyst and 50 °C as 5.43 kg PE $(\text{mmol Ni})^{-1} \text{h}^{-1}$, *i.e.*, 0.543 kg PE $(\text{mmol Ni})^{-1} \text{h}^{-1} \text{bar}^{-1}$, whereas switching to CC 2000 and MAO cocatalyst gave a value of 0.715 kg PE $\text{mmol}^{-1} \text{Ni h}^{-1} \text{bar}^{-1}$ [7]. These were the only two sets of conditions in that report. The performance of this catalyst in ethylene polymerization with MAO over a relatively wide range of experimental factors, especially CC, was investigated. The effect of factor variations and also their interactions on responses (activity, MW, and crystallinity) were studied and visualized via RSM. Furthermore, a slightly different synthesis of the complex is reported, as is its crystallization and full structural characterization by single-crystal X-ray diffraction.

Experimental

Materials

All manipulations of air or moisture sensitive compounds were carried out under an inert atmosphere using standard Schlenk line technique. Polymerization grade ethylene with high purity was obtained from Bandar Imam Petrochemical Corporation (BIPC, Iran) and was further purified by passage through an oxygen/moisture trap. Toluene for polymerization was obtained from Bandar Imam Petrochemical Corporation (BIPC, Iran) and was refluxed in the presence of calcium hydride and distilled prior to use (water content was lower than 5 ppm by Karl–Fischer titration). Tetrahydrofuran (THF) and diethylether were purchased from Merck (Germany) and distilled from sodium/benzophenone prior to use. Dichloromethane (DCM) was purchased from Fluka (Switzerland) and dried over CaH_2 . MAO was

purchased from Aldrich (USA) as a 10 wt% solution in toluene and used as received. Acenaphthenequinone and ethylene glycol dimethyl ether nickel(II) bromide complex ((DME)NiBr₂) were purchased from Aldrich and used without purification. 2,6-Diisopropylaniline and 2,4,6-trimethylaniline were purchased from Aldrich and refluxed over calcium hydride prior to use.

Synthesis

Synthesis of ((2,6-diisopropylphenyl)imino)-acenaphthene (A1). In modification of the literature procedures [7, 19], an ethanol (80 mL) solution of acenaphthenequinone (4 g, 0.02 mol) was treated with 1 mL of formic acid, followed by slow, dropwise addition (over approx. 8 h) of a solution of 2,6-diisopropylaniline (3.76 mL, 0.02 mol) in 50 mL of ethanol. The resulting mixture was stirred at 60 °C (over 8 h), cooled to room temperature, and filtered to remove unreacted acenaphthenequinone. The filtrate was cooled to -10 °C overnight. The red-orange solid that deposited was filtered, washed with ether, and dried to yield 3.6 g (45%) of product.

¹H NMR (250 MHz, CDCl₃, δ) 8.18–8.22 (dd, 2H, acenaphthene protons), 8.0 (d, 1H, acenaphthene protons), 7.84 (t, 1H, acenaphthene protons), 7.42 (t, 1H, acenaphthene protons), 7.27 (m, 3H, aromatic protons), 6.61 (d, 1H, acenaphthene protons), 2.38 (hep, 2H, CH(CH₃)₂), 1.15, 0.82 (2d, 12H, CH(CH₃)₂). ¹³C NMR (100 MHz, CDCl₃, δ selected resonances) 189.87 (C=O), 160.52 (C=N), 28.31 (CH(CH₃)₂), 23.39, 23.12 (CH(CH₃)₂). IR (KBr): 1425.41, 1652.33 cm⁻¹ (C=N), 1724.47 cm⁻¹ (C=O). Its spectroscopic data matched that given in the literature [7].

Synthesis of ((2,6-diisopropylphenyl)imino)-((2,4,6-trimethylphenyl)imino)-acenaphthene (A2). In modification of a literature procedure [7], a solution of A1 (1 g, 3.10 mol), 2,4,6-trimethylaniline (0.54 mL, 3.36 mol) and a catalytic amount of *p*-toluenesulfonic acid in THF (60 mL) was refluxed for 17 h in the presence of molecular sieves (4 Å). The mixture was filtered, concentrated *in vacuo*, and the resulting oily compound was dissolved in dichloromethane (40 mL). This solution was washed twice with 1 M NaOH (20 mL) and three times with saturated NaCl solution (20 mL). The solution was dried on MgSO₄, filtered, and concentrated, yielding a red powder. Yield: 51%. The crude product was dried and purified by column chromatography (ethyl acetate:hexane = 1 : 4, including 2% triethylamine, silica gel) to afford 0.5 g of red solid (m.p.: 258–260 °C, yield = 39%).

¹H NMR (250 MHz, CDCl₃, δ) 7.86–7.91 (dd, 2H, acenaphthene protons), 7.33–7.44 (2pst, 2H, acenaphthene protons), 7.26 (m, 3H, aromatic protons), 6.98 (s, 2H, aromatic protons), 6.75 (d, 1H, acenaphthene protons), 6.62 (d, 1H, acenaphthene protons), 3.0 (hep, 2H, CH(CH₃)₂), 2.38 (s, 3H, para-CH₃), 2.21 (s, 6H, meta-CH₃), 1.21, 0.96 (2d, 12H, CH(CH₃)₂). ¹³C NMR (100 MHz, CDCl₃, selected resonances δ) 161.50, 160.90 (C=N), 28.41 (CH(CH₃)₂), 23.27, 22.95 (CH(CH₃)₂), 20.81, 17.53 (CH₃). IR (KBr): 1425.41, 1652.33 cm⁻¹ (C=N). Spectroscopic data matched that reported [7].

Synthesis of [2,6-diisopropylphenylimino)-((2,4,6-trimethylphenyl)imino)-acenaphthene nickel(II) dibromide (C1). In a slight modification of the literature procedure, which was recently reported [7], (DME)NiBr₂ (0.12 g, 0.40 mmol), A2 (0.20 g, 0.44 mmol), and CH₂Cl₂ (12 mL) were placed in a Schlenk flask under nitrogen and the reaction mixture

was stirred at room temperature for 24 h. The solvent was evaporated *in vacuo*. The solid was washed three times with Et₂O (10 mL) and dried *in vacuo* to afford red-brown powder (yield: 80%). Anal. calcd for C₃₃H₃₄N₂Br₂Ni: C, 58.52; H, 5.02; N, 4.14. Found: C, 58.37; H, 4.86; N, 4.09. A crystalline sample of **C1** suitable for X-ray diffraction studies was obtained by vapor diffusion of hexane into a DCM solution under non-anhydrous conditions.

Crystallographic data

Crystallographic data for the structure of **C1** have been deposited at the Cambridge Crystallographic Data Center, CCDC 1023990, deposition@ccdc.cam.ac.uk, <http://www.ccdc.cam.ac.uk/deposit>, Telephone: (44) 01223 762910, Facsimile: (44) 01223 336033, Postal Address: CCDC, 12 Union Road, Cambridge CB2 1EZ, UK.

Ethylene polymerization procedure

The polymerizations were carried out in a 300-mL stainless steel reactor containing systems for full control of temperature and reaction pressure. The reactor was repeatedly evacuated and refilled with argon and finally filled with ethylene gas (1 bar). It was then charged with toluene (150 mL) and MAO, and its temperature was set. The catalyst was dissolved in 3 mL of toluene under a dry nitrogen atmosphere and transferred into the reactor. Immediately, the reactor was pressurized and then the solution stirred for 1 h. The polymerization was terminated by venting unreacted monomer and adding 10 vol. % HCl/methanol solution (80 CC). The polymer was washed with an excess of methanol and dried in vacuum at 40 °C overnight.

Response surface experimental design

The ethylene polymerization performance of **C1** was statistically analyzed through the RSM, based on Box–Behnken design. The factors or independent variables were temperature (x_T : levels 10, 30, 50 °C), ethylene pressure (x_P : levels 3, 5, 7 bar), and cocatalyst-to-catalyst ratio (CC) (x_C : levels 100, 1550, 3000), whereas the response or independent variable was catalyst activity, MW, and crystallinity. The temperature and pressure were selected based on previous reported results with nickel(II) systems [7, 19, 26–32]. The levels of CC were selected based on a group of polymerization runs, detailed in the ethylene polymerization section. The experimental plan generated using Minitab[®] 15 software involved 13 runs. Also, to provide an estimate of the experimental error in the process and achieve more precise estimates of the factor effects, the center point, that is, the midpoint between the high and low levels, was replicated twice. Therefore, in total, the software suggested 15 test runs, as detailed in the ethylene polymerization section.

Characterization

The ¹H and ¹³C NMR data of the organic compounds were obtained on a Bruker (Germany) Avance 250 MHz spectrometer at ambient temperature and CDCl₃ as a solvent.

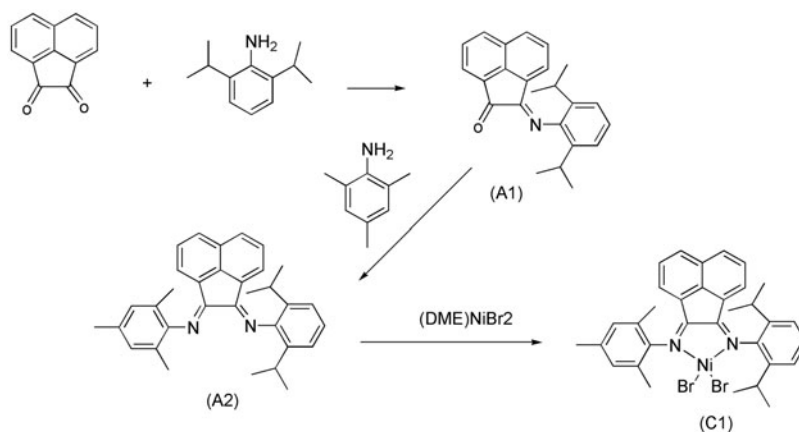
IR spectra were recorded on a Perkin–Elmer (USA) SpectrumRX1 Fourier transform infrared spectrometer using Nujol mulls between KBr plates. Elemental analysis measurements were performed on a CHNSO Elemental Analyzer (Germany) Vario ELIII. Single

crystals were mounted in perfluoropolyether oil into an Oxford Instruments Cryostream (UK) 700. Diffraction measurements were performed on an Oxford Diffraction X-Calibur 2 diffractometer using graphite-monochromated Mo-K α radiation, and the data were collected and processed by CrysAlis PRO and CrysAlis RED (Oxford Diffraction Ltd., Abingdon, UK, 2007). The structure was solved using SHELXS86 and refined with SHELXL [33]. The DSC measurements were performed on a Mettler-Toledo (Switzerland) model 822^c instrument, interfaced to a digital computer equipped with Star E 9.01 software (Sencor FRS5) at a heating/cooling rate of 10 °C min⁻¹. Samples were heated from room temperature to 170 °C and held there for 2 min, followed by cooling to -120 °C. Finally, they were reheated to 170 °C and the melting point and crystallinity were determined according to the results obtained from the final step. The molecular weights and the molecular weight distributions of the polymer samples were determined at 145 °C with a Varian (USA) PL-GPC120 high-temperature chromatograph. Trichlorobenzene was employed as the solvent and calibration was made by polystyrene standard.

Results and discussion

Synthesis and structure of the complex

The low-symmetry diimine compound **A2** was obtained in two steps as shown in scheme 2. The mono aryl imino acenaphthene **A1** was synthesized by condensation of the acenaphthenequinone with 2,6-diisopropylaniline in ethanol. The resulting product was further reacted with 2,4,6-trimethylaniline in THF in the presence of a catalytic amount of *p*-toluenesulfonic acid and molecular sieves (4 Å) to remove the water formed during the condensation reaction. The crude product was purified using column chromatography, followed by recrystallization to obtain *bis* aryl imino acenaphthene **A2**. Its synthesis has also recently been independently reported by Redshaw, Sun and coworkers [7], although solvent choice was different. We chose lower-boiling solvents in order to lower the reaction temperature, and hence amounts of acenaphthenequinone substituted with two identical



Scheme 2. Synthesis procedure of **A2** and **C1**.

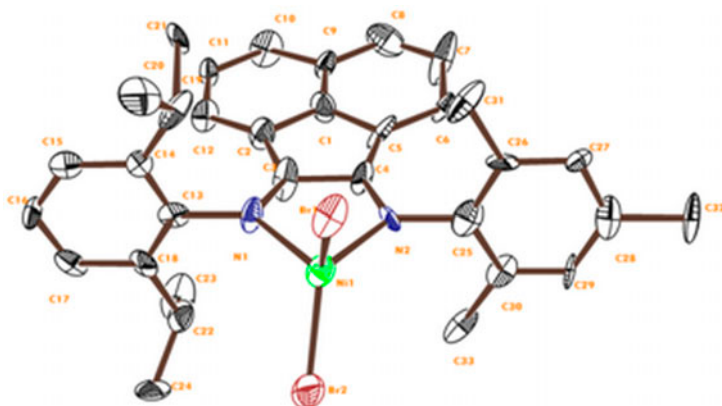


Figure 1. ORTEP representation of the crystal and molecular structure of **C1** at 60% probability. Hydrogens have been omitted for clarity.

anilines. This could have occurred in the first step via over-reaction, or in the second step via statistical scrambling of the two anilines, since the imine formation is in equilibrium. However, where there is a large steric mismatch between the two anilines, this is not thought to be a serious problem, as reflected in the fact that the other reported synthesis is in fact higher-yielding and did not require chromatography [7].

The synthesis of **C1** by addition of **A2** to (DME)NiBr₂ is depicted in scheme 2. Crystallization from DCM allowed isolation of the product as red-brown crystals in 80% yield. Single crystals of **C1** suitable for X-ray diffraction studies were obtained by vapor diffusion of hexane into a DCM solution under non-anhydrous conditions. The resulting molecular structure is shown in figure 1.

The crystallographic parameters, crystal data, and refinement details are summarized in tables 1 and 2, respectively. The molecular structure features a distorted tetrahedral geometry, similar to other published examples, notably **C3**, which differs from **C1** only in the absence of the *p*-Me group from one aryl. Consequently, **C1** and **C3** are very nearly isotopic and isostructural [7]. This comparison is complicated somewhat by the fact that **C1** was solved and refined in *P2₁/c*, the standard setting of space group No. 14, whereas **C3** was set in the alternative *P2₁/n*. However, transposing the published cell dimensions of **C3** to *P2₁/c* gives the values *a*: 10.642, *b*: 20.891, and *c*: 15.788 Å, β = 124.70, remarkably close to those of **C1**. The cell lengths *a* and *b* are essentially identical, as is the angle β , but there is a lengthening of approximately 1 Å along *c* caused by the presence of the extra methyl group in **C1**, as is expected given the orientation of the molecules in the cell approximately parallel to the *c* axis.

The aryl rings of the α -diimine lie nearly perpendicular to the plane formed by the metal and coordinated nitrogens, the diisopropyl-substituted ring being closer to perpendicular (89°) than the trimethyl one (79°), as for **C3** [7]. This slight skewing of the trimethyl-substituted ring is accompanied by a twisting of the Br₂Ni plane relative to the N₂Ni plane. The bond distances in the X-ray structure of **A2** reveal that the Ni(1)-N(1) is longer than Ni(1)-N(2) by 0.063(9) Å, an amount which is on the edge of what may be considered chemically significant, most likely due in part to the greater steric repulsion from the more heavily substituted aromatic ring. This difference is greater, however, than that recorded for **C3** (0.010

Table 1. Crystallographic data for unsymmetrical catalyst **C1**.

Empirical formula	C ₃₃ H ₃₄ Br ₂ N ₂ Ni
Formula weight	677.15
Temperature	100(2) K
Wavelength	0.71 Å
Crystal system	Monoclinic
Space group	<i>P</i> 2 ₁ / <i>c</i> , <i>Z</i> = 4
Unit cell dimensions	<i>a</i> = 10.624(7) Å <i>b</i> = 20.543(13) Å <i>c</i> = 16.627(12) Å α = 90.00° β = 123.461(13)° γ = 90.00°
Absorption coefficient	3.305 mm ⁻¹
<i>F</i> (0 0 0)	1376
Theta range for data collection	1.77 to 28.38°
Index ranges	-13 ≤ <i>h</i> ≤ 13, -27 ≤ <i>k</i> ≤ 27, -22 ≤ <i>l</i> ≤ 22
Reflections collected	23,971
Completeness to theta	93.9% (to θ = 28.38°)
Refinement method	Full-matrix least-squares on <i>F</i> ²
Data/restraints/parameters	7137/24/350
Goodness of fit on <i>F</i> ²	0.611
Final <i>R</i> indices [<i>I</i> > 2σ(<i>I</i>)]	<i>R</i> 1 = 0.0648, <i>wR</i> 2 = 0.1076
<i>R</i> indices (all data)	<i>R</i> 1 = 0.3660, <i>wR</i> 2 = 0.1446
Largest diff. peak and hole	0.567 and -0.755 e Å ⁻³

Table 2. Selected bond distances and angles (Å, °) for **C1**.

Br1–Ni1	2.340(2)	Ni1–N2	1.989(9)
Br2–Ni1	2.333(3)	Ni1–N1	2.052(9)
N2–Ni1–N1	82.0(4)	N2–Ni1–Br1	104.0(3)
N2–Ni1–Br2	117.4(3)	N1–Ni1–Br1	109.8(3)
N1–Ni1–Br2	110.0(3)	Br2–Ni1–Br1	125.23(10)

(4) Å), by a statistically significant amount [7]. Thus, it seems that there is a just-perceptible electronic structural effect in that the electron-pushing *p*-Me group makes N2 a marginally better σ -donor than N1. These marginal structural changes result in detectable variations in polymerization activity and branching rate, however (*vide infra*). To summarize, catalyst **C1** shares a pseudo-tetrahedral structure [7] with **C3** and **C4** and several other NiBr₂ complexes of diimines, but not all: even restricting comparisons to other cases bearing an acenaphthene backbone, there are several cases where dimeric five-coordinate structures with bridging bromides are found, even among bulkier cases such as **C2** [34].

Ethylene polymerization

Selection of CC levels

The catalytic behavior of **C1** was evaluated in the presence of MAO, as for most previously reported nickel(II) α -diimine-based catalytic systems. It has been reported that low-symmetry catalysts such as **C3** and **C4**, just as for other nickel(II) α -diimine complexes such as **C2**, performed better (higher activity, lower branching) at lower temperature and higher pressure [3].

Most previous reports include an assessment of the effect of CC on activity via trials of limited ranges [4, 6–9]. For example, Guo, Sun, and Glaser report an optimum of CC equal to 3000 from the range 2000 to 3500 [9]. In other similar cases [7], a range of 1500–2500 produced an optimum of 2000. Much lower ratios have occasionally been found possible, especially with non-MAO activators [28]. Therefore, it is considered that an important parameter to vary in assessing any polyethylene precatalysts is CC. For **C1**, the activity was evaluated at constant levels of temperature and pressure (30 °C and 7 bar) while varying CC from 100 to 3000. Figure 2 illustrates the ethylene polymerization activity of **C1** versus CC. It shows that although variation of activity with CC is not especially dramatic at lower levels of CC (1000–3000), it is at higher levels. Hence, a wide range of CC was selected for evaluation of **C1** in ethylene polymerization.

Estimated regression models

The results of the performance evaluation of **C1** according to the experimental plan are shown in table 3. The behavior of the system was explained by the following second-degree polynomial equation (equation 1):

$$R = b_0 + \sum_{i=1}^n b_i x_i + \sum_{i=1}^n b_{ii} x_i^2 + \sum_{i < j}^n b_{ij} x_i x_j \quad (1)$$

where R denotes the predicted response of the process, x_i refers to the coded factors (temperature, x_T , ethylene pressure, x_P and cocatalyst-to-catalyst ratio, x_C), and b_0 , b_i , b_{ii} , b_{ij} are regression coefficients. Reducing equation (1) led to three partial quadratic models for the responses of activity (R_A), weight-average molecular weight (R_{MW}), and crystallinity (%) (R_{XII}), as shown in equations (2)–(4), respectively.

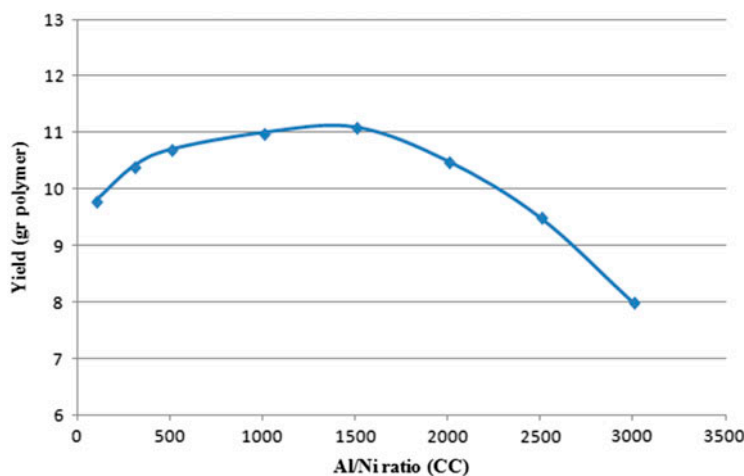


Figure 2. Effect of cocatalyst-to-catalyst ratio on the activity of MAO-activated **C1**. Polymerization at $T = 30$ °C, $p = 7$ bar, $t = 1$ h.

Table 3. Performance of C1/MAO in ethylene polymerization^a.

Experimental run	Independent variables (factors)			Activity (kg mol ⁻¹ Ni ⁻¹ h ⁻¹)	MW (g mol ⁻¹)	PDI	Crystallinity (%)
	x _T (°C)	x _P (bar)	x _{CC}				
1	10	3	1550	3400	520,800	2.72	35.97
2	50	3	1550	3333.3	81,173	2.09	16
3	10	7	1550	5000	505,507	2.92	46.29
4	50	7	1550	3936.6	68,189	2.18	17.22
5	10	5	100	3966.6	497,079	2.72	54.34
6	50	5	100	3156.5	74,619	2.12	22.39
7	10	5	3000	3133.3	399,324	2.73	43.85
8	50	5	3000	2363.3	79,090	2.08	17.59
9	30	3	100	2033.3	171,374	3.30	28.47
10	30	7	100	3050	474,409	2.77	46.81
11	30	3	3000	2333.3	229,904	2.93	25.59
12	30	7	3000	2800	220,873	3.58	25.30
13	30	5	1550	2833.3	190,000	2.78	25.10
14	30	5	1550	3066.6	206,182	3.07	29.36
15	30	5	1550	3466.6	172,186	2.69	29.89

^aPolymerization condition: time of polymerization = 1 h, [Ni] = 3 μmol.

$$R_A = 3182 - 338.8x_T - 460.8x_P - 197.1x_C + 690.6x_T^2 - 672.8x_C^2 - 249.2x_Tx_P - 137.5x_Px_C \quad (2)$$

$$R_{MW} = 189456 - 202451x_T + 33216x_P - 36033x_C + 46421x_T^2 + 58040x_P^2 + 26641x_C^2 - 78017x_Px_C \quad (3)$$

$$R_{xtl} = 27.27 - 13.15x_T + 3.94x_P - 4.96x_C + 1.73x_T^2 + 4.90x_C^2 - 2.77x_Tx_P - 4.65x_Px_C \quad (4)$$

Details of the statistical basis for exclusion of non-significant terms (p -values higher than 0.05) and evaluation of the goodness of fit of the reduced regression models (F value and analysis of variance (ANOVA) table) is detailed in Supplementary Material.

The estimated regression coefficients for the above models are presented in table 4. Table 5 shows the ANOVA table at a 95% confidence level. In the activity regression model (equation 2), the significant coefficients are x_T , x_P , x_T^2 and x_C^2 because their p -values are less than 0.05 (table 4). The suggested model for the activity variations was deemed adequate because not only was the F value for the regression model greater than F_{tab} but also the F value for the lack-of-fit was less than F_{tab} (table 4). Probability plots of residual distribution for the regression models are presented in figure 3. According to figure 3(a), the p -value for the Anderson-Darling test is higher than the chosen significance level (usually 0.05), which supports the normal distribution of residuals and adequacy of the activity fitted model [35–38].

In the MW regression model (equation 3), all of the coefficients are significant except x_C^2 and x_T^2 . The fitted model was adequate because the F value for the regression model was more than F_{tab} and F value for the lack-of-fit was less than F_{tab} (table 4). Figure 3(b) indicates the model has an adequate goodness of fit.

Table 4. Estimated regression coefficients for various regression models.

Terms of the models	Activity		MW		Crystallinity	
	Coefficient	<i>p</i> -value	Coefficient	<i>p</i> -value	Coefficient	<i>p</i> -value
x_t	-338.8	0.018	-202,451	0.000	-13.156	0.000
x_p	460.8	0.004	33,216	0.006	3.949	0.006
x_c	-197.1	0.117	-36,033	0.002	-4.960	0.002
x_c^2	690.6	0.004	46,421	0.282	1.732	0.282
x_p^2	-	-	58,040	0.013	-	-
x_c^3	-672.8	0.004	26,644	0.094	4.905	0.013
$x_p x_p$	-249.2	0.154	-	-	-2.775	0.094
$x_t x_c$	-	-	-	-	-	-
$x_p x_c$	-137.5	0.408	-78,017	0.014	-4.658	0.014

Table 5. ANOVA table for the regression models.

Source	Activity				MW				Crystallinity			
	DF	<i>F</i>	<i>F</i> _{tab.}	<i>p</i> -value	DF	<i>F</i>	<i>F</i> _{tab.}	<i>p</i> -value	DF	<i>F</i>	<i>F</i> _{tab.}	<i>p</i> -value
Regression	7	10.22	3.78	0.003	7	19.87	3.78	0.0	7	33.49	3.78	0.0
Residual error	7				7				7			
Lack-of-fit	5	0.93	19.29	0.591	5	13.24	19.29	0.072	5	1.26	19.29	0.49
Pure error	2				2				2			
Total	14				14				14			

In the crystallinity regression model (equation 4), significant coefficient-related terms include x_t , x_{cc} , x_p , x_c^2 and $x_p x_c$. The fitted model was adequate according to F value data in table 4. Also according to figure 3(c), the residuals follow a normal distribution. The above models could be shown as 3-D surface plots, representing the trend of response variations with factors. Figure 4 shows the surface and contour plots of activity variation of MAO-activated catalyst **C1** according to equation 2. Figure 4(a) and (c) shows that there is a second-order variation of activity with temperature at all levels of CC and pressure. It depicts that activity passes through a minimum at 30 °C but the maximum activity appears at 10 °C. This is surprising, since in other Ni(II) acenaphthenediimine-based polyethylene catalysts, though at higher temperatures activity is impeded by reduced ethylene solubility and catalyst deactivation, in the low-temperature regime normal Arrhenius rate increase with temperature has been observed, a fact attributed to lower activation energies for monomer propagation than for catalyst deactivation [24, 25], leading to optima commonly in the 20–30 °C temperature range. The fact that the optimum temperature is as low as 10 °C for **C1** suggests that it is more susceptible than some catalysts to deactivation processes. If those processes were reductive in nature, then the electron-pushing *p*-Me group on one aryl may account for promotion of such a reductive deactivation, through increased donation to Ni(II). This may explain the lower-temperature optimum than that found for otherwise identical **C3** (20 °C) [19]. Conversely, lower optimum temperatures have been found for phenanthrene-based ligands, where the larger polyaromatic core facilitates ligand-reduction processes [16]. Furthermore, a catalyst bearing a less-reducible β-triimine ligand with trimethyl-phenyl substituents, yielded a higher optimal temperature of 30 °C [26]. The idea that deactivation processes are reductive in nature also fits well with the known reducing character of Me₃Al present in MAO, and thereby also goes some way to explaining the

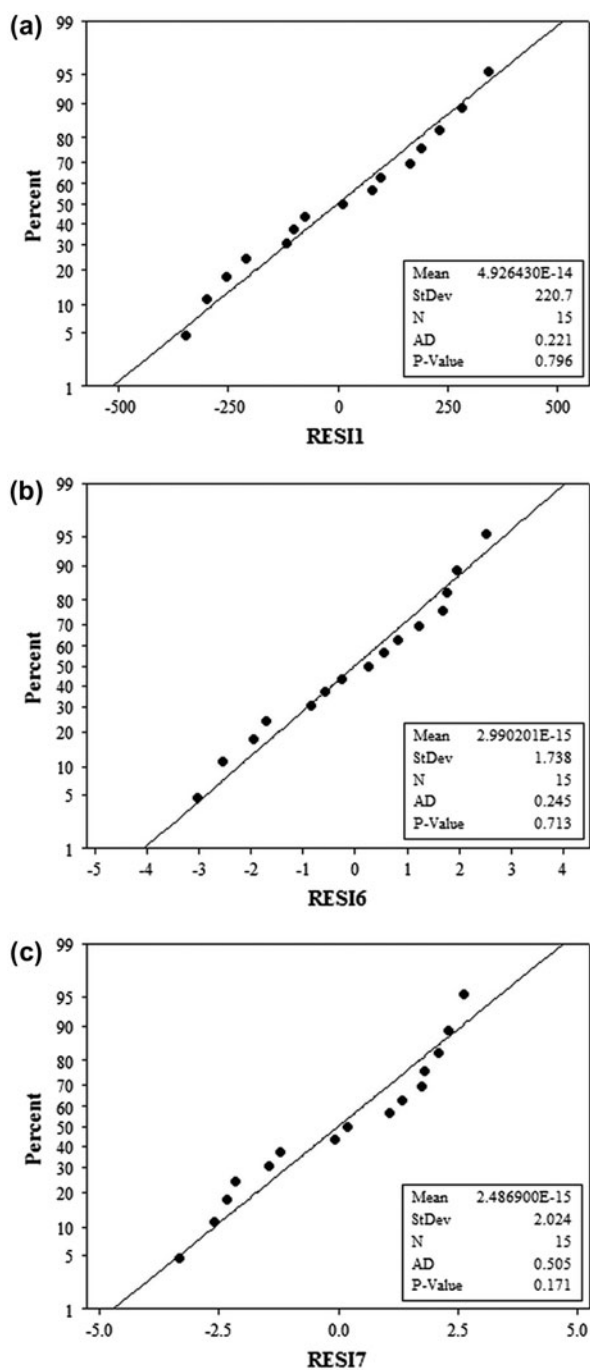


Figure 3. Probability plots of residual distribution for the regression models of (a) activity, (b) MW, and (c) crystallinity.

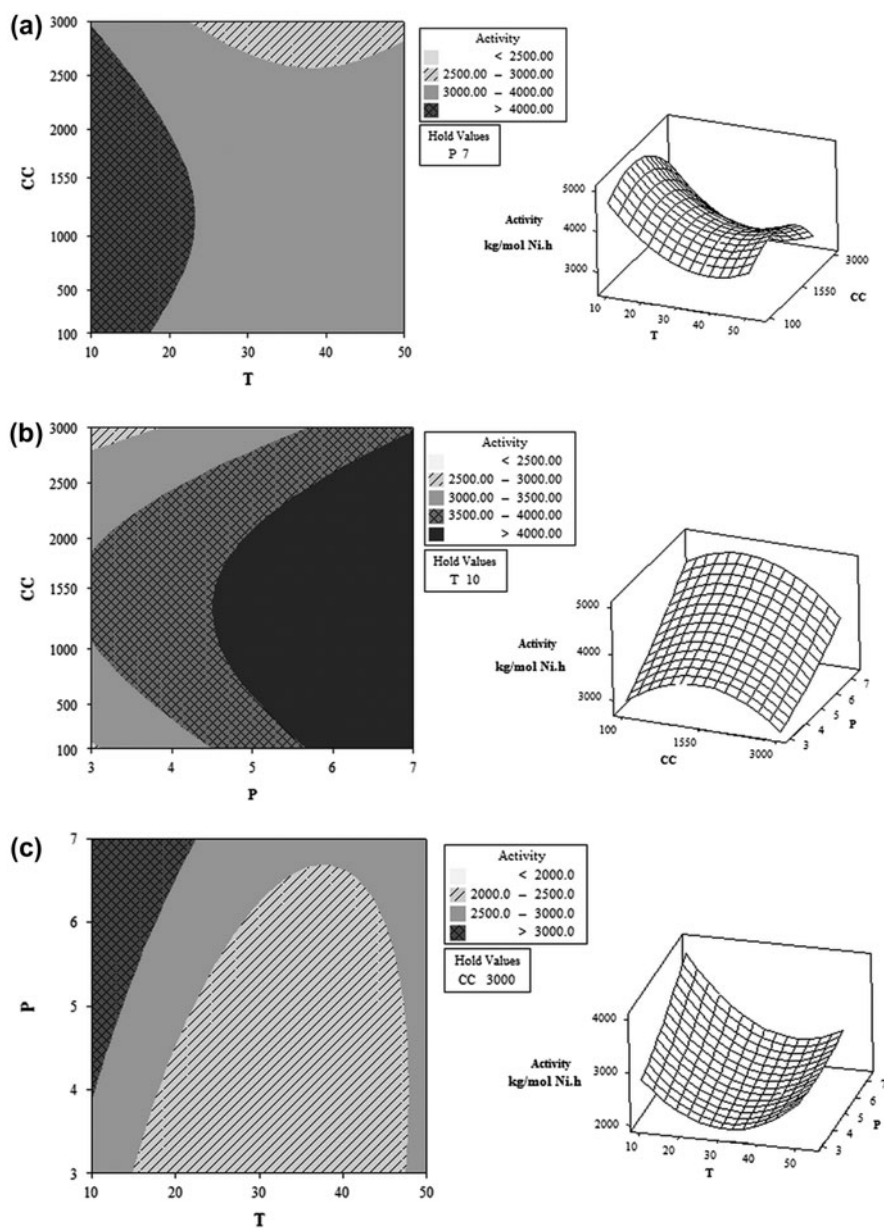


Figure 4. Surface and contour plots of activity variation for MAO-activated C1 as a function of (a) temperature and CC, (b) pressure and CC, and (c) temperature and pressure.

negative effect of CC being too high (*vide infra*). It is also apparent from figure 4(b) and (c) that pressure has a linear effect on activity at all temperatures, with the steepest gradient at lower temperatures due to the lower solubility of gasses at higher temperatures. At this range of monomer concentration, the rate of polymerization is first order with respect to monomer pressure. Hence, it is instructive to use units normalized to 1 bar pressure when

comparing activities between groups or within a set where pressure is a variable: The highest activity found under those terms was in fact that of run 1, reaching $3.4 \text{ kg PE mmol}^{-1} \text{ Ni h}^{-1}$ at 3 bar, *i.e.*, $1.13 \text{ kg PE mmol}^{-1} \text{ Ni h}^{-1} \text{ bar}^{-1}$ collected at CC equal to 1550 and 10°C . This value compares with $0.715 \text{ kg PE (mmol Ni)}^{-1} \text{ h}^{-1} \text{ bar}^{-1}$ for C3 at 10 bar, CC

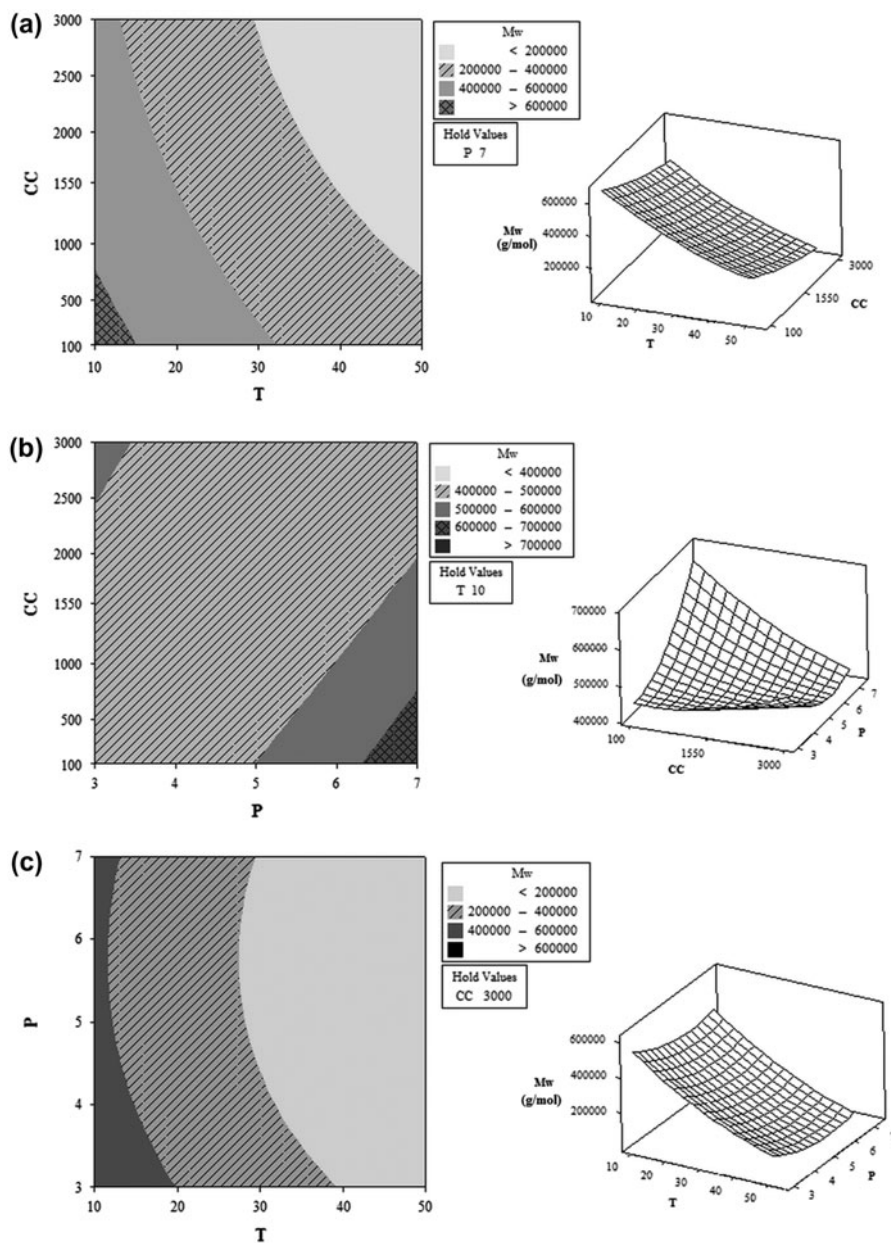


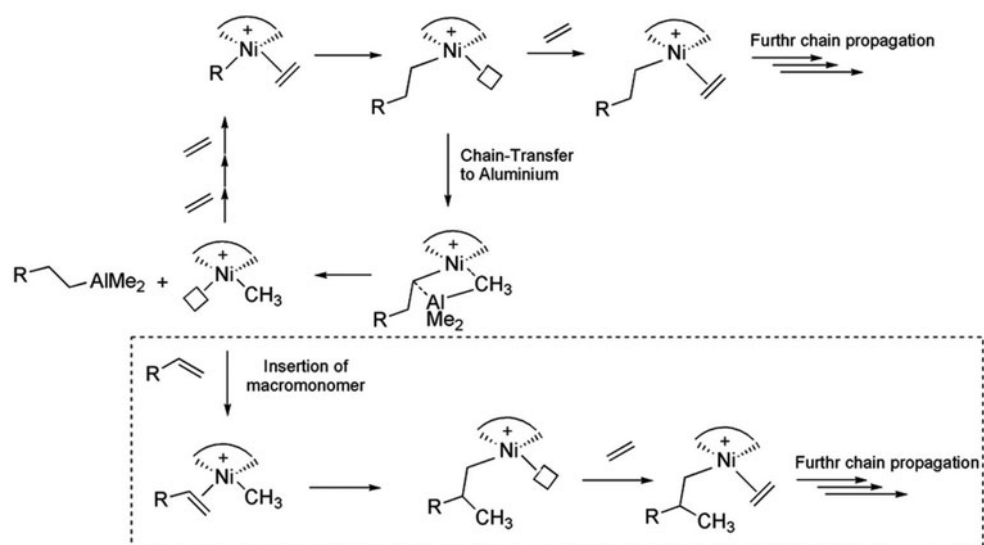
Figure 5. Surface and contour plots of MW variation for polymers prepared with MAO-activated C1 as a function of (a) temperature and CC, (b) pressure and CC, and (c) temperature and pressure.

equal to 2000 and 20 °C, though that run was for 30 min rather than the full 1 h runs used here [7]. Furthermore, **C1** under those conditions gave a similar value, 0.715 kg PE mmol⁻¹ Ni h⁻¹ bar⁻¹ for **C3** at 10 bar, 30 min run [7]. This value would appear to be in broad agreement with the models shown, when corrected for the shorter run-time. An even higher pressure-corrected value has been reported for **C3** at 15 min runtime, 3.15 kg PE (mmol Ni)⁻¹ h⁻¹ bar⁻¹ at 1.25 bar [19], underlining the fact that though activity does vary linearly with pressure, the gradient is less than unity. However, the main point to be deduced from these literature comparisons must be that though there are small effects on activity, MW and branching rate with the *p*-Me variation of **C1** versus **C3** and in other such cases [7, 28–30], the effects of run-time and pressure on such values are much greater [3].

According to figure 4(a) and (b), there is a non-linear variation of activity with CC; it passes through a maximum at CC equal to 1550. This implies that below a threshold of molar ratio of cocatalyst to catalyst (CC < 1550), there might be a hindrance of efficient activation of catalyst, due to slow alkylation reactions or to insufficient Al-alkyl scavenging effects. But also, exceeding this ratio facilitates dialkylation of the nickel centers. Such nickel-dialkyl intermediates deactivate rapidly by reductive elimination to nickel(0). Another explanation for decreasing activity of catalyst in high levels of CC is deactivation by reaction of the imine ligand fragments with Me₃Al [39].

The maximum activity (absolute, not corrected for pressure) of **C1** (4960 kg PE (mol Ni)⁻¹ h⁻¹) with full 1-h run appears at 10 °C after raising ethylene pressure and CC to 7 bar and 1550, respectively. Higher pressure runs give higher maxima [40, 41].

Figure 5 shows the surface and contour plots of MW variation for polymers prepared with MAO-activated **C1**. The MW decreases sharply as the temperature increases [figure 5(a) and (c)]. It is likely that the rate of chain transfer increases with increasing temperature [24, 39] passing through a minimum at 5 bar. These observations probably suggest that at low levels of CC, chain transfer both to monomer and to aluminum is slow, whereas at high



Scheme 3. Possible chain transfer and chain propagation pathways in ethylene polymerization of MAO-activated **C1**.

levels of CC chain transfer to Al dominates. That it should show such dependence on pressure is surprising, perhaps increase in pressure causes an increase in rate of the associative reaction needed to facilitate chain transfer to aluminum, until such point that the concentration of ethene inhibits coordination of organoaluminum.

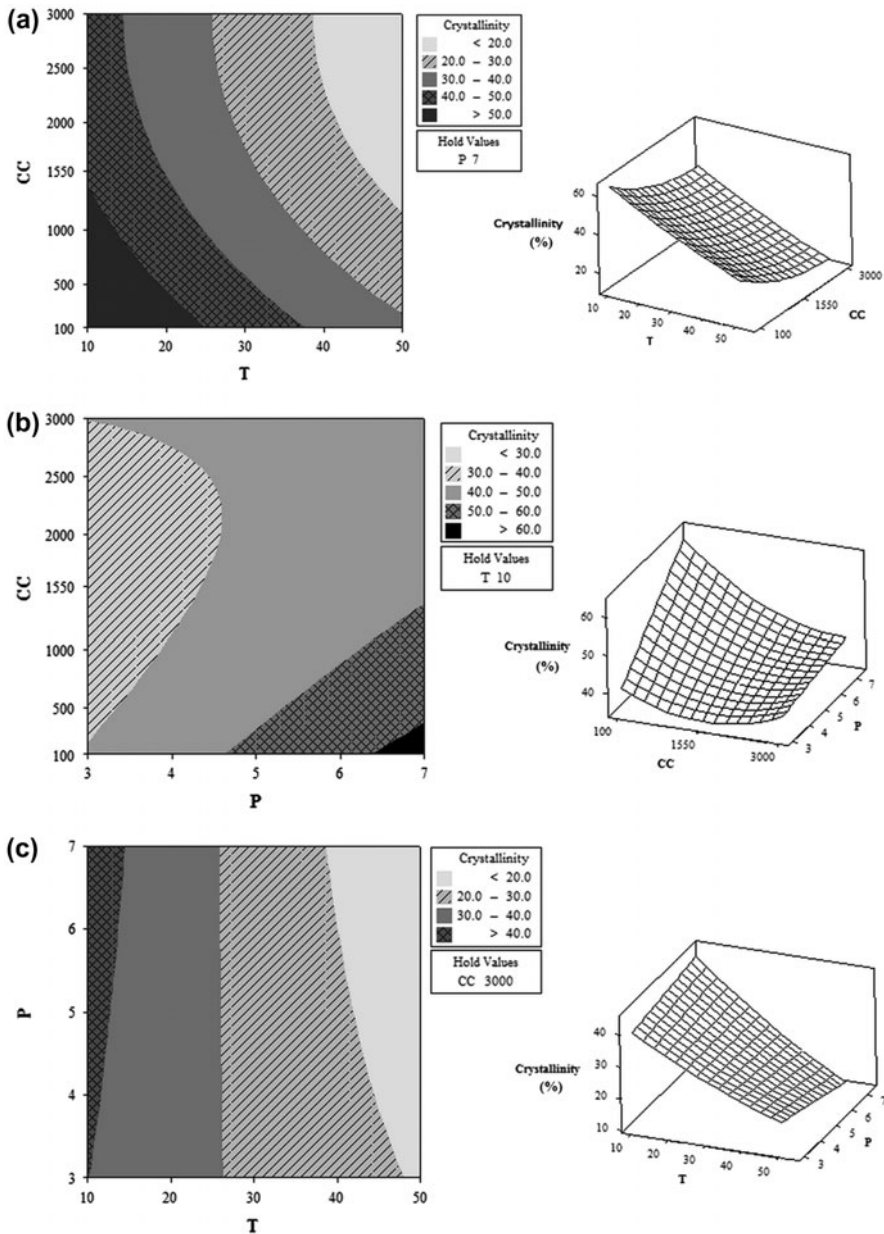


Figure 6. Surface and contour plots of crystallinity variation for polymer produced with MAO-activated C1 as a function of (a) temperature and CC, (b) pressure and CC, and (c) temperature and pressure.

The importance of chain transfer to aluminum depends on the concentration of Me_3Al , which acts as a chain transfer agent. At low levels of CC, because of the low concentration of Me_3Al , the rate of chain transfer to aluminum is negligible but at higher levels, there is a competition between chain transfer to aluminum and insertion of previously formed oligomer or macromonomer [39]. The possible chain transfer and propagation pathways for this system are shown in scheme 3 [41, 42]. Maximum MW ($666,342 \text{ g mol}^{-1}$) is achieved at 10°C , 7 bar and CC equal to 100 [figure 5(b)]. This observation is in accord with previous reports that decreasing steric bulk in the axial sites lead to an increase in the rate of chain termination relative to the rate of propagation [25]. It is significant to note that molecular weight distribution (PDI) of polymers produced at 50°C is narrower than that found at 10°C (table 3). This could be explained by the greater degree of branching and lower molecular weights of polymers produced at 50°C , which lead to more homogeneous systems [21].

Figure 6 shows the surface and contour plots of crystallinity variation for polymers prepared with MAO-activated **C1**. It is clear that a higher level of crystallinity is obtained at lower temperatures [figure 6(a) and (c)], implying that the chain-walking process which results in short-chain branches is suppressed relative to linear propagation at lower temperatures [33, 35], in line with its higher activation energy. There is a linear variation of crystallinity with pressure [42, 43]. In other words, the polyethylenes obtained under higher pressures are characterized by a more linear and less branched structure due to an increased rate of trapping and insertion relative to the rate of chain walking [32].

Within the broad range of CC studied, the variation of crystallinity is more significant at lower levels of CC [figure 6(b)]. For example at 10°C and CC equal to 100, the crystallinity increases from 40 to 63% with increasing pressure from 3 to 7 bar, but at CC equal to 3000 it is just from 40 to 44%. This suggests that higher levels of aluminum may somewhat impede access of ethylene to the active site, thereby favoring the branching reaction over linear monomer enchainment.

The maximum crystallinity level (about 63%) implies that it should prove possible to reach linear polymers (<5 branch per thousand carbons) with melt transition between 125 and 135°C at 10°C , 7 bar and CC equal to 100. In comparison with the literature, these results show that the electronic nature of the *para* substituent does not have a major effect on the branching degree of the resulting polymers [21, 22].

Conclusion

The low-symmetry nickel(II) α -diimine **C1** was structurally characterized by single-crystal X-ray diffraction then used as catalyst precursor on ethylene polymerization in the presence of MAO. RSM was applied to analyze the effect of polymerization conditions (temperature, monomer pressure, and CC) and their interactions on activity, MW, and crystallinity of polymer. The maximum activity of **C1** was achieved at 10°C , although there was an increase of activity from 30 to 50°C . It revealed that for every single catalytic system, there is a competition between propagation and deactivation rates that lead to maximum productivity at a specific temperature. For example, greater degrees of *ortho*-steric encumbrance, via dibenzhydryl [44] or cyclophane [45] substituents, can increase optimum temperature as high as 90°C , though in the dibenzhydryl case the steric encumbrance is so great that activity suffers (only $0.08 \text{ kg (mmol Ni)}^{-1} \text{ h}^{-1} \text{ bar}^{-1}$, at 6.9 bar over a 15 min run) [44], while

for the cyclophane case claims are made of levels of activity which challenge those of the most active of early transition metal catalysts [45, 46], $3.04 \text{ kg (mmol Ni)}^{-1} \text{ h}^{-1} \text{ bar}^{-1}$, though this value relates to a $30 \text{ }^\circ\text{C}$, 13.8 bar run terminated after the most active first 5 min, rather than the full 1-h runs reported here which give rise to values approximately one third of this. It is likely that overall activities are broadly comparable. Returning to the results specific to **C1**, the obtained surface and contour plots showed that CC had a pronounced effect on responses. At high levels of CC, excessive complexation of MAO with active centers led to the decrease of activity. Also there was an increase of MW with pressure at high levels of CC, but it showed second-order variation at lower levels.

A linear increase of polymer crystallinity with pressure was observed, as noted before [3, 26], but more intriguing is the fact that the effect was more significant at lower levels of CC. This suggests that MAO may impede access of monomer at high CC. Moreover, the *para* substituent on the arylimino ring did not majorly affect the branching content of final polymers, in contrast to findings in other cases [30].

It can be concluded that polymer properties cannot be optimized without considering the interaction of polymerization factors, which are critical to the ultimate catalyst performance. It was also found that properties of final product could be controlled by tuning the reaction conditions, a conclusion which has for nickel been known qualitatively since early work [1–3], but which can best be visualized and modeled quantitatively using RSM [26, 27]. Further studies on nickel-catalyzed polymerizations may benefit from similar treatment of all relevant variables using RSM.

Acknowledgments

We are grateful to Dr Omar Alsayari for advice on synthesis of **C1**, growth of crystals of **C1** and helpful discussions during his stay in Manchester University. We are also grateful to Dr James Raftery for collection, solution, and refinement of the X-ray data for **C1**.

Disclosure statement

No potential conflict of interest was reported by the authors.

Supplemental data

Supplemental data for this article can be accessed here [<http://dx.doi.org/10.1080/00958972.2015.1057130>].

References

- [1] L.K. Johnson, C.M. Killian, M. Brookhart. *J. Am. Chem. Soc.*, **117**, 6414 (1995).
- [2] M. Brookhart, L.K. Johnson, C.M. Killian, S. Mecking, D.J. Tempel. *Polym Prep.*, **37**, 254 (1996).
- [3] S.D. Ittel, L.K. Johnson, M. Brookhart. *Chem. Rev.*, **100**, 1169 (2000).
- [4] H. Liu, W. Zhao, X. Hao, C. Redshaw, W. Huang, W.H. Sun. *Organometallics*, **30**, 2418 (2011).
- [5] M. Schmid, R. Eberhardt, M. Klinga, M. Leskelä, B. Rieger. *Organometallics*, **20**, 2321 (2001).

- [6] H. Liu, W. Zhao, J. Yu, W. Yang, X. Hao, C. Redshaw, L. Chen, W.H. Sun. *Catal. Sci. Technol.*, **2**, 415 (2012).
- [7] S. Kong, K. Song, T. Liang, C.Y. Guo, W.H. Sun, C. Redshaw. *Dalton Trans.*, **42**, 9176 (2013).
- [8] D. Jia, W. Zhang, W. Liu, L. Wang, C. Redshaw, W.H. Sun. *Catal. Sci. Technol.*, **23**, 2737 (2013).
- [9] S. Kong, C.Y. Guo, W. Yang, L. Wang, W.H. Sun, R. Glaser. *J. Organomet. Chem.*, **725**, 37 (2013).
- [10] M. Helldörfer, J. Backhaus, W. Milius, H.G. Alt. *J. Mol. Catal. A: Chem.*, **193**, 59 (2003).
- [11] F.S. Liu, H.B. Hu, Y. Xu, L.H. Guo, S.B. Zai, K.M. Song, H.Y. Gao, L. Zhang, F.M. Zhu, Q. Wu. *Macromolecules*, **42**, 7789 (2009).
- [12] C.S. Popeney, Z. Guan. *Organometallics*, **24**, 1145 (2005).
- [13] C.S. Popeney, Z. Guan. *Macromolecules*, **43**, 4091 (2010).
- [14] J. Liu, Y. Li, Y. Li, N. Hu. *J. Appl. Polym. Sci.*, **109**, 700 (2008).
- [15] L.K. Johnson, S. Mecking, M. Brookhart. *J. Am. Chem. Soc.*, **118**, 267 (1996).
- [16] L. Li, M. Jeon, S.Y. Kim. *J. Mol. Catal. A: Chem.*, **303**, 110 (2009).
- [17] B.C. Peoples, G.D. Vega, C. Valdebenito, R. Quijada, A. Ibañez, M. Valderrama, R. Rojas. *J. Organomet. Chem.*, **700**, 147 (2012).
- [18] F.S. Liu, H.B. Hu, Y. Xu, L.H. Guo, S.B. Zai, K.M. Song, H.Y. Gao, L. Zhang, F.M. Zhu, Q. Wu. *Macromolecules*, **42**, 7789 (2009).
- [19] M. Jeon, S.Y. Kim. *Polym. J.*, **40**, 409 (2008).
- [20] M.M. Wegner, A.K. Ott, B. Rieger. *Macromolecules*, **43**, 3624 (2010).
- [21] G.J.P. Britovsek, V.C. Gibson, D.F. Wass. *Angew. Chem.*, **111**, 448 (1999).
- [22] G. Mao, Y. Jiang, N. Li, Q. Wang, D. Zheng, M. Li, Y. Ning. *Chin. Sci. Bull.*, **59**, 2505 (2014).
- [23] S. Mecking, L.K. Johnson, L. Wang, M. Brookhart. *J. Am. Chem. Soc.*, **120**, 888 (1998).
- [24] L. Deng, P. Margl, T. Ziegler. *J. Am. Chem. Soc.*, **119**, 1094 (1997).
- [25] L. Deng, T.K. Woo, L. Cavallo, P. Margl, T. Ziegler. *J. Am. Chem. Soc.*, **119**, 6177 (1998).
- [26] N. Ghasemi Hamedani, H. Arabi, G.H. Zohuri, F.S. Mair, A. Jolleys. *J. Polym. Sci., Part A: Polym. Chem.*, **51**, 1520 (2013).
- [27] H. Arabi, M.S. Beheshti, M. Yousefi, N. Ghasemi Hamedani. *Polym. Bull.*, **70**, 2765 (2013).
- [28] H. Liu, W. Zhao, X. Hao, C. Redshaw, W. Huang, W.H. Sun. *Organometallics*, **30**, 2418 (2011).
- [29] M. Schmid, R. Eberhardt, J. Kukral, B. Rieger. *Z. Naturforsch. B: Chem. Sci.*, **57b**, 1141 (2002).
- [30] J. Yuan, F. Song, J. Li, Z. Jia, F. Wang, B. Yuan. *Inorg. Chim. Acta*, **400**, 99 (2013).
- [31] W. Sun, W. Zhang, H. Lih. Patent WO 2012122854 (Institute of Chemistry, Chinese Academy of Sciences) (2012).
- [32] O. Alsayari. Group 4 and group 10 post metallocene ethylene polymerization catalysts: Catalyst structure-polymer properties relationship. PhD thesis, The University of Manchester (2010).
- [33] G. Sheldrick. *Acta Crystallogr. A*, **64**, 112 (2008).
- [34] (a) J.O. Liimatta, B. Löfgren, M. Miettinen, M. Ahlgren, M. Haukka, T.T. Pakkanen. *J. Polym. Sci., Part A: Polym. Chem.*, **39**, 1426 (2001); (b) R.J. Maldanis, J.S. Wood, A. Chandrasekaran, M.D. Rausch, J.C.W. Chien. *J. Organomet. Chem.*, **645**, 158 (2002); (c) H.R. Liu, P.T. Gomes, S.I. Costa, M.T. Duarte, R. Branquinho, A.C. Fernandez, J.C.W. Chien, R.P. Singh, M.M. Marques. *Appl. Organomet. Chem.*, **690**, 1314 (2005); (d) F. Wang, J. Yuan, Q. Li, R. Tanaka, Y. Nakayama, T. Shiono. *Appl. Organomet. Chem.*, **28**, 477 (2014); (e) C. Wen, S. Yuan, Q. Shi, E. Yue, D. Liu, W.-H. Sun. *Organometallics*, **33**, 7223 (2014).
- [35] I. Xiarchos, A. Jaworska, G. Zakrzewska-Trznadel. *J. Membr. Sci.*, **321**, 222 (2008).
- [36] M. Ahmadi, R. Ranjani, M. Nekoomanesh, G. Zohuri, H. Arabi. *Iran Polym. J.*, **16**, 133 (2007).
- [37] L.C. Ferreira Jr., P.A. Melo Jr., G.L. Crossetti, G.B. Galland, M. Nele, J.C. Pinto. *Polym. Eng. Sci.*, **50**, 1797 (2010).
- [38] M. Vatankehah, S. Pourmahdian, F. Afshar. *Iran Polym. J.*, **20**, 897 (2011).
- [39] L.C. Simon, C.P. Williams, J.B.P. Soares, R.F. De Souza. *J. Mol. Catal. A: Chem.*, **165**, 55 (2001).
- [40] J.D. Azoulay, Z.A. Koretz, G. Wu, G.C. Bazan. *Angew. Chem. Int. Ed.*, **49**, 7890 (2010).
- [41] D.P. Gates, S.A. Svejda, E. Oñate, C.M. Killian, L.K. Johnson, P.S. White, M. Brookhart. *Macromolecules*, **33**, 2320 (2000).
- [42] P.H.M. Budzelaar. *Comput. Mol. Sci.*, **2**, 221 (2012).
- [43] F. AlObaidi, Z. Ye, S. Zhu. *Polymer*, **45**, 6823 (2004).
- [44] J.L. Rhinehart, N.E. Mitchell, B.K. Long. *ACS Catal.*, **4**, 2501 (2014).
- [45] D.H. Camacho, E.V. Salo, J.W. Ziller, Z. Guan. *Angew. Chem., Int. Ed.*, **43**, 1821 (2004).
- [46] H.G. Alt, A. Köppl. *Chem. Rev.*, **100**, 1205 (2000).